Arch. Pharm. Chem. Life Sci. 2017, *350*, e1600351

ARCH PHARM
Archiv der Pharmazie

Full Paper

Mannich-Benzimidazole Derivatives as Antioxidant and Anticholinesterase Inhibitors: Synthesis, Biological Evaluations, and Molecular Docking Study

Ayşe Selcen Alpan[1], *Görkem Sarıkaya*[1], *Güneş Çoban*[1], *Sülünay Parlar*[1], *Güliz Armagan*[2], *and Vildan Alptüzün*[1]

[1] Faculty of Pharmacy, Department of Pharmaceutical Chemistry, Ege University, Bornova, Izmir, Turkey
[2] Faculty of Pharmacy, Department of Biochemistry, Ege University, Bornova, Izmir, Turkey

A series of Mannich bases of benzimidazole derivatives having a phenolic group were designed to assess their anticholinesterase and antioxidant activities. The acetylcholinesterase (AChE) and butyrylcholinesterase (BuChE) inhibitory activities were evaluated *in vitro* by using Ellman's method. According to the activity results, all of the compounds exhibited moderate to good AChE inhibitory activity (except for **2a**), with IC_{50} values ranging from 0.93 to 10.85 μM, and generally displayed moderate BuChE inhibitory activity. Also, most of the compounds were selective against BuChE. Compound **4b** was the most active molecule on the AChE enzyme and also selective. In addition, we investigated the antioxidant effects of the synthesized compounds against $FeCl_2$/ascorbic acid-induced oxidative stress in the rat brain *in vitro*, and the activity results showed that most of the compounds are effective as radical scavengers. Molecular docking studies and molecular dynamics simulations were also carried out.

Keywords: Antioxidant activity / Benzimidazole / Cholinesterase inhibitors / Mannich bases / Molecular modeling

Received: November 24, 2016; Revised: March 15, 2017; Accepted: March 16, 2017

DOI 10.1002/ardp.201600351

Additional supporting information may be found in the online version of this article at the publisher's web-site.

Introduction

Alzheimer's disease (AD) is an age-related neurodegenerative disorder of the brain affecting many elderly people. It is characterized by a progressive neurodegeneration, impairment in cognition and memory loss, ultimately leading to death of the patient [1]. According to World Alzheimer Report in 2010, more than 30 million people worldwide suffer from AD and this number is expected to reach more than 100 million in 2050 [2].

Correspondence: Dr. Ayşe Selcen Alpan, Faculty of Pharmacy, Department of Pharmaceutical Chemistry, Ege University, Ankara Street, No: 172/98, 35040 Bornova, Izmir, Turkey.
E-mail: selcen.alpan@ege.edu.tr
Fax: +90-232-3885258

The etiology of AD is not yet fully understood, but common hallmarks, such as intracellular tau-protein aggregation, extracellular beta-amyloid (Aβ) plaques, the selective loss of cholinergic neurons, and increased oxidative stress are considered key pathological features of the disease [3].

Based on the "cholinergic hypothesis" the level of acetylcholine (ACh) neurotransmitter which is responsible for cholinergic transmission is reduced at the cholinergic synapses. Current therapy of AD include the enhancement of the central cholinergic function by increasing the concentration of ACh in the synaptic cleft via inhibition of AChE as well as BuChE which are involved in the breakdown of ACh [4–7]. Up to date, the only five drugs approved by Food and Drug Administration (FDA) are four cholinesterase inhibitors named tacrine, donepezil, rivastigmine, galantamine, and a *N*-methyl-D-aspartate (NMDA) receptor antagonist memantine. All of them, except tacrine, are still in clinical use. As a result, both AChE and BuChE enzymes are the most promising approach for the treatment of AD [8].

ARCH PHARM
Archiv der Pharmazie

Another hypothesis was reported that oxidative stress plays a vital role in the pathogenesis of AD [9, 10]. Lowered antioxidant capacity of the brain progresses the neurodegeneration. It is important to improve the antioxidant defense system of the brain tissue against the oxidative stress which has a role in the neurodegenerative diseases. Decreasing the oxidative stress and improving the antioxidant defense is reported to be effective to slow down the early and progressive stages of the AD, also antioxidants are found to have neuroprotective effects [11–13]. Reactive oxygen species as superoxide, hydroxyl, and peroxyl radicals are causes of the oxidative stress associated with the pathogenesis of AD. It is known that antioxidants which include phenols and aromatic amines that break chains by reactions with peroxyl radicals. Tocopherol, *p*-coumaric acid, ferulic acid, and caffeic acid are the best known antioxidant agents having phenolic group. On the other hand, many of compounds bearing benzimidazole ring system have been reported to possess antioxidant activity [14, 15].

The benzimidazole ring system is a molecular pattern to produce biologically active compounds and has significant importance in medicinal chemistry. Benzimidazole derivatives have many biological activities, such as antibacterial [16], anticancer [17], antimicrobial [18], anthelmintic [19], antihypertensive [20], antiviral [21], antifungal [22], anti-HIV [23], and DNA topoisomerase inhibitory [24] and also this heterocyclic system has been used as a skeleton to discover new compounds with cholinesterase inhibitory activity [25].

The Mannich reaction is an important method for synthesis of novel compounds. This reaction is useful for preparing many drug molecules which contain aminoalkyl chain. Mannich bases have been reported as very reactive and recognized to possess potent diverse activities [26]. The Mannich synthesis introduces a basic function which can render the molecule soluble in aqueous solvents when it is transformed into the aminium salt. Therefore Mannich bases are prepared to improve the pharmacokinetic properties of the compounds. Mannich base derivatives of benzimidazoles play an important role in medicinal chemistry with so many pharmaceutical importances [27].

Due to the multi-pathogenesis of AD, designing new multi-target anti-AD agents rather than single-target drugs would be useful in the treatment and management of AD. In this context and with these ideas, a series of some Mannich bases of benzimidazole derivatives having phenolic group were designed and synthesized. Then, they were evaluated for their possible *in vitro* antioxidant and AChE/BuChE inhibitory potentials.

Results and discussion

Chemistry

In this study, 4-(1*H*-benzo[*d*]imidazol-2-yl)-2-[(substituted-amine)methyl]phenol types of Mannich bases **1a–4d** were designed and synthesized by starting from 4-(1*H*-benzimidazole-2-yl)phenol derivatives (**1–4**). Dimethylamine (**a**), diethylamine (**b**), pyrrolidine (**c**), piperidine (**d**) were used as an amine compound (Scheme 1).

All the Mannich bases derivatives were reported for the first time in this study except for **1a**, **1c**, and **1d** [28]. The chemical structures of the compounds were confirmed by IR, ^{1}H NMR, ^{13}C NMR, ESI-MS, and elemental analysis. IR spectral bands obtained in solid phase at 2400–3200 cm^{-1} are characteristic of benzimidazole derivatives [29]. According to the IR spectra of the Mannich bases of benzimidazole derivatives having phenolic group, O–H and N–H stretching bands were observed at 3689–3570 cm^{-1} and 3474–3232 cm^{-1}. Moreover, the IR

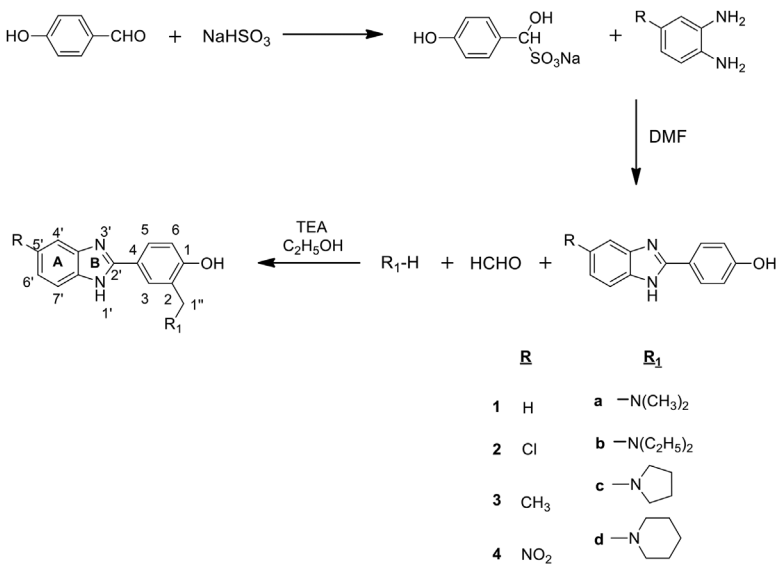

Scheme 1. The synthesis pathway of Mannich bases of benzimidazole derivatives having phenolic group.

spectra of the title compounds include strong/medium bands in the 1685–1426 cm^{-1} region and correspond to the C=C and C=N stretching vibrations. The stretching bands corresponding to benzenoid ring were confirmative values with the literature survey [30]. The assessment of the chemical shifts in ^1H NMR spectrum demonstrated that the aromatic and aliphatic protons were observed in the expected regions with expected multiplicities confirming the substitution patterns. ^1H NMR data of the nonsubstituted benzimidazole compounds (**1a–d**) showed a 1,2-disubstituted benzene system at the A ring of the benzimidazole nucleus and a ABX-substituted benzene system due to the *p*-hydroxyphenyl substituent at 2-position of ring B. The aromatic proton signals of *p*-hydroxyphenyl substituent at 2-position were observed within prospective chemical shift values and divisions while the hydrogen atoms of 1*H*-benzimidazole ring at 4- and 7-positions were not detected at the prospective divisions. The lack of H atom signals on ^1H NMR spectra and the lack of the signals belonging to the 3a, 4, 7, and 7a C atoms in the ^{13}C NMR spectra are noteworthy as it may suggest a proton exchange due to 1,3-tautomerization [31]. ^{13}C NMR spectral results were assigned by using the 2D HSQC technique and the spectral data of our previous study [25b].

Biological activities

AChE/BuChE inhibitory activity

AChE and BuChE inhibitory activities of target compounds were determined by the method of Ellman et al. [32]. Tacrine and galanthamine were used as the reference compounds. IC_{50} values of the compounds are summarized in Table 1.

Among all the Mannich bases, **4b** was the most active compound against AChE while **4c** exhibited the highest inhibitory activity against BuChE, also both of them contain nitro group at 5-position of benzimidazole ring. Moreover, **4b** with IC_{50} value of 0.93 μM presented a noteworthy AChE inhibitory activity compared to the galanthamine ($IC_{50} = 0.43$ μM), and **4c** showed higher inhibition ($IC_{50} = 6.27$ μM) than galanthamine ($IC_{50} = 14.92$ μM) on BuChE enzyme.

According to activity results, the intermediate compounds which were not substituted with Mannich bases except for **4** showed better inhibition on BuChE enzyme than AChE. In contrast, the inhibitory potency shifted from BuChE to AChE by the addition of Mannich bases to the intermediate compounds except for **2a** and **2c**. With regard to the AChE activity results, while the **b** series (diethyl derivatives) displayed the best inhibitory activity within the substituted amine derivatives, the **c** series (**b** series cyclized derivatives) exhibited remarkably low inhibitory activity. Conversely, the pyrrolidine series showed higher inhibition potency than diethyl series against BuChE. On the other hand, compared to the substituents at 5-position of benzimidazole ring, the Mannich bases bearing nitro substituent displayed the highest inhibition on AChE.

Regarding the BuChE activity results, all compounds showed moderate to weak BuChE inhibiting property. When final compounds were evaluated for their inhibitory potency, the highest activity at pyrrolidine derivatives, the lowest activity at dimethyl derivatives were observed.

Concerning the AChE versus BuChE selectivity in the final compounds, while **c** series gave values of the similar magnitude, the **b** series showed the highest selectivity.

Table 1. ***In vitro*** **inhibition[Q2] of AChE and BuChE.**

	$IC_{50} \pm$ SEM (μM)[a]		
	AChE	BuChE	Selectivity BuChE/AChE
1	17.33 ± 0.27	4.59 ± 7.34	0.3
1a	6.70 ± 0.07	>100	
1b	4.11 ± 0.10	26.92 ± 0.37	6.55
1c	8.28 ± 1.40	11.08 ± 0.40	1.34
1d	6.26 ± 0.44	14.85 ± 0.38	2.37
2	14.59 ± 1.13	8.52 ± 1.89	0.6
2a	57.78 ± 3.46	29.62 ± 0.38	0.51
2b	2.36 ± 0.04	19.80 ± 1.41	8.39
2c	10.85 ± 0.87	9.54 ± 3.45	0.88
2d	4.92 ± 7.73	7.90 ± 0.33	1.61
3	15.93 ± 0.78	4.67 ± 3.39	0.3
3a	7.30 ± 0.17	51.83 ± 1.50	7.10
3b	1.14 ± 0.08	26.45 ± 0.57	23.20
3c	8.51 ± 0.72	8.80 ± 0.83	1.03
3d	2.13 ± 0.10	8.95 ± 0.32	4.20
4	35.44 ± 0.73	>100	
4a	5.30 ± 0.31	55.38 ± 3.87	10.45
4b	0.93 ± 0.04	12.72 ± 0.25	13.68
4c	4.21 ± 0.19	6.27 ± 0.24	1.49
4d	1.61 ± 0.15	10.47 ± 0.11	6.50
Tacrine	0.075 ± 0.02	0.0098 ± 0.0002	
Galanthamine	0.43 ± 0.03	14.92 ± 0.57	

[a] Data are means ± standard error of the mean of triplicate independent experiments.

Reactive oxygen species (ROS) and lipid peroxidation inhibition

In recent studies, it was shown that Fe^{2+} and ascorbic acid induce lipid peroxidation and protein oxidation *in vitro* [33]. In the current study, we investigated antioxidant effects of Mannich bases derivatives against $FeCl_2$/ascorbic acid-induced oxidative stress in the rat brain *in vitro*. The *in vitro* antioxidant effects of the novel compounds on rat brain lipid peroxidation levels and their free radicals scavenging properties were investigated and compared with *tert*-butyl hydroquinone (tBHQ) (Tables 2 and 3). tBHQ is a synthetic phenolic antioxidant and effective in protecting against cellular dysfunction induced by oxidative stress [34]. In our study, we used tBHQ to compare the effectiveness of compounds in oxidative stress condition. All compounds, except compounds **2** and **2b** at 10^{-4} M concentration, showed a dose-dependent inhibition of the $FeCl_2$-ascorbic acid stimulated lipid peroxidation in the brain homogenate. They had an inhibitory effect in the range of 10–35% at 10^{-4} M concentration and 10–20% at 10^{-5} M and 10^{-6} M

Table 2. The inhibitory effects of the synthesized compounds on lipid peroxidation in rat brain homogenates.

	% Lipid peroxidation inhibition		
	10^{-6} M	10^{-5} M	10^{-4} M
1	14.19 ± 0.05	20.16 ± 1.19	31.69 ± 0.68
1a	16.58 ± 0.012	20.56 ± 1.52	27.71 ± 3.65
1b	13.00 ± 1.19	15.78 ± 1.68	28.11 ± 1.82
1c	21.75 ± 3.01	25.33 ± 0.68	34.47 ± 3.61
1d	16.98 ± 2.49	18.22 ± 1.38	18.57 ± 3.44
2	17.77 ± 1.19	21.35 ± 1.19	n.s.
2a	13.80 ± 0.83	19.76 ± 1.38	26.52 ± 0.68
2b	18.57 ± 2.75	17.37 ± 3.01	n.s.
2c	15.78 ± 1.38	20.56 ± 3.44	7.04 ± 1.31
2d	14.99 ± 3.02	14.19 ± 2.12	23.34 ± 3.64
3	17.38 ± 1.82	15.78 ± 1.82	13.80 ± 1.88
3a	16.18 ± 0.68	17.40 ± 1.51	22.15 ± 1.82
3b	13.39 ± 0.64	20.16 ± 2.38	20.95 ± 3.83
3c	14.60 ± 1.82	15.39 ± 1.19	28.11 ± 1.82
3d	17.77 ± 1.19	19.00 ± 4.30	23.34 ± 5.63
4	11.81 ± 1.19	18.12 ± 2.01	26.18 ± 2.48
4a	16.98 ± 3.83	13.89 ± 1.57	13.80 ± 2.12
4b	18.57 ± 1.44	21.99 ± 2.12	28.51 ± 1.19
4c	13.40 ± 1.82	22.94 ± 3.02	18.17 ± 2.48
4d	16.98 ± 3.44	20.95 ± 2.77	33.28 ± 1.19

Table 3. The effects of synthesized compounds on ROS production in rat brain homogenates.

	% Inhibition in ROS production		
	10^{-6} M	10^{-5} M	10^{-4} M
1	10.55 ± 0.96	31.84 ± 4.67	34.32 ± 4.98
1a	40.14 ± 2.25	20.86 ± 2.36	22.07 ± 2.46
1b	28.93 ± 1.45	26.94 ± 2.51	22.42 ± 3.45
1c	6.66 ± 0.12	14.90 ± 0.47	n.s.
1d	32.89 ± 4.69	32.76 ± 4.58	33.85 ± 3.69
2	34.38 ± 2.58	24.43 ± 2.14	29.27 ± 2.56
2a	7.11 ± 0.56	16.01 ± 1.46	25.22 ± 1.89
2b	35.99 ± 4.12	28.19 ± 1.85	26.35 ± 1.96
2c	18.96 ± 2.36	26.75 ± 3.47	33.69 ± 4.81
2d	n.s.	3.41 ± 0.58	n.s.
3	n.s.	3.54 ± 0.14	7.20 ± 0.94
3a	42.57 ± 1.58	37.73 ± 4.74	26.39 ± 2.69
3b	39.64 ± 3.51	43.58 ± 5.69	42.85 ± 5.89
3c	n.s.	10.39 ± 1.53	12.61 ± 1.47
3d	15.62 ± 1.25	26.47 ± 3.98	37.81 ± 4.86
4	n.s.	14.69 ± 1.11	26.84 ± 3.64
4a	41.81 ± 2.36	36.04 ± 3.65	19.73 ± 3.56
4b	31.73 ± 3.47	35.88 ± 2.56	25.06 ± 2.87
4c	53.09 ± 4.56	20.68 ± 2.45	18.60 ± 1.98
4d	31.17 ± 5.42	43.34 ± 5.41	33.32 ± 3.87

n.s., non-significant.
All samples were measured in triplicate.

concentrations. Only compound **2c** at 10^{-4} M concentration showed less than 10% inhibitory effect on lipid peroxidation (7%). Moreover all compounds had a higher inhibitory effect on ROS production at the 10^{-4} M concentration. tBHQ was used as an antioxidant in this model and caused 30% inhibition of lipid peroxidation at 50 μM concentration and 20.86% inhibition of ROS production in rat brain homogenate. Comparison of the activity results revealed that the compounds are nearly equally active with tBHQ. These results support the idea that these compounds are effective as radical scavengers and may be considered as important agents for combating oxidative damage in brain.

Docking studies

Molecular docking is the beneficial technique that enables to evaluate the interactions between drug candidates and their target proteins theoretically. In our study, molecular docking was performed to determine non-covalent interactions of benzimidazole derivatives in the gorge of active site of AChE (PDB id: 1EVE resolved at 2.5 Å) and homology model of *eq*BuChE built from *hu*BuChE (PDB id: 4TPK), respectively. For this purpose, benzimidazole derivatives were docked in order to detect their binding geometry and affinity in the gorge of active site of AChE and BuChE using Gold 5.2.1 program. The scoring values and docking poses of the best ranked docking solutions of the titled compounds are reported in Table 4 and Supporting Information Tables S1 and S2. Before the docking study of the title compounds, in order to validate docking methods, donepezil as well-known AChE inhibitor and the inhibitor compound as 2-naphthamide derivative taken from the crystal structure of BuChE (PDB id: 4TPK) were docked in AChE and homology model of BuChE, respectively. The best ranked docking poses and the scoring values of the known inhibitors inside the title proteins were figured and reported in Supporting Information Figs. S1, S2 and Tables S1, S2. In addition to this, 2D structure and IUPAC name of the inhibitor compound as 2-naphthamide derivative are given in Supporting Information Fig. S2. As a results of docking study of inhibitor compounds, the best ranked docking pose of donepezil was observed occupying peripheral site of AChE with both the acyl-binding and the quaternary ammonium binding site on the active site of *ee*AchE the same as the crystal structure of donepezil complex with AChE (PDB id: 1EVE) (Supporting Information Fig. S1). A similar situation was observed in the docking study of the inhibitor compound as 2-naphthamide derivative inside homology model of BuChE. The best ranked docking pose of 2-naphthamide derivative was determined settling down into homology model of BuChE as same as 2-naphthamide derivative-*hu*BuChE complex (PDB id: 4TPK) (Supporting Information Fig. S2). In addition to this, the comparison of the first ranked solutions of donepezil and compound **4b** and crystal form of donepezil inside AChE and the comparison of the first ranked solutions of 2-naphthamide derivative and compound **4b** inside homology model and crystal form of 2-naphthamide derivative

Table 4. Docking scores for Mannich benzimidazole derivatives inside AChE (PDB id:1EVE) and BuChE, using Goldscore.

Compounds	AChE (1EVE) Goldscore	BuChE (homology model) Goldscore	LogP (o/w)	SLogP
1a	67.3894 (1)	65.6682 (1)	3.0580	1.8464
1b	71.0066 (1)	61.6776 (1)	3.7400	2.6266
1c	69.9121 (1)	65.1086 (1)	3.5900	2.3806
1d	73.9542 (1)	68.2961 (1)	4.0320	2.7707
2a	70.1304 (1)	63.2620 (1)	3.6870	2.4998
2b	73.0449 (1)	62.1830 (1)	4.3690	3.2800
2c	73.3679 (1)	61.6921 (1)	4.2190	3.0340
2d	74.9947 (1)	62.9659 (1)	4.6610	3.4241
3a	70.4602 (1)	63.5189 (1)	3.3930	2.1548
3b	74.3062 (1)	57.6974 (1)	4.0750	2.9350
3c	71.1790 (1)	62.9501 (1)	3.9250	2.6890
3d	77.4958 (1)	60.0787 (1)	4.3670	3.0791
4a	72.6672 (1)	62.6701 (1)	3.0300	1.7546
4b	77.7039 (1)	62.4717 (1)	3.7120	2.5348
4c	73.7197 (1)	60.4329 (1)	3.5620	2.2888
4d	80.2573 (1)	63.5915 (1)	4.0040	2.6789

The absolute ranking positions for the suggested binding poses are given inside brackets. Calculated LogP (octanol/water) and SLogP values.

inside crystal form of BuChE are given in Supporting Information Figs. S1 and S2, respectively.

As a result of biological activity study, compound **4b** has the best inhibitory potency on AChE among the studied compounds. While the best ranked docking pose of compound **4b** is evaluated, the pose of title compound seems settling into both the acyl-binding and the quaternary ammonium binding site in the active site of AChE (Fig. 1). 5-Nitro-substituted benzimidazole ring of compound lies on the quaternary ammonium binding domain of the catalytic site of AChE formed by amino acid residues Trp84 and Tyr130. Beside of this, 4-hydroxyphenyl group of compound **4b**

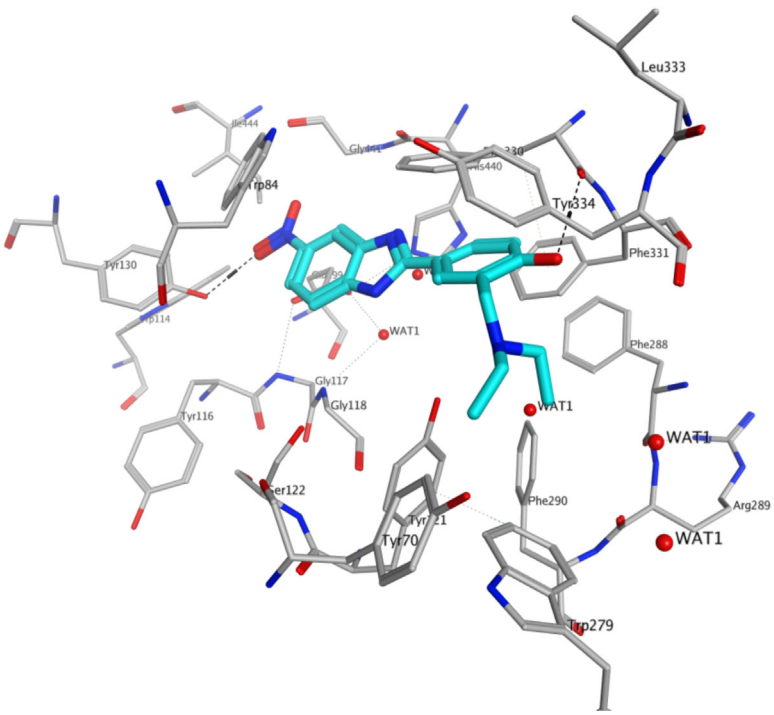

Figure 1. The first ranked solution of compound **4b** using Goldscore in AChE (PDB id: 1EVE). Residues and water molecules are named using three-letter code and specifier. Cyan and white sticks represent compound **4b** and the active site residues, respectively. For clarity, all hydrogen atoms have been removed. H bonds and CH–π interactions are represented by black and green dashed lines, respectively.

occupies hydrophobic pocket formed by amino acid residues Tyr121, Phe290, Phe330, Phe331, and Tyr334 at the catalytic site of enzyme (Fig. 1). Lastly, the positively charged tertiary amine group of compound goes toward the peripheral site of AChE, but it is not able to arrive at this site.

As the best ranked docking pose of compound **4b** in the gorge of BuChE is viewed, compound **4b** occurs occupying the catalytic site of titled enzyme. 4-Hydroxyphenyl group of compound **4b** is oriented toward the catalytic triad formed by Ser198, Glu325, and His438. In addition to this, benzimidazole ring of compound **4b** settles between the acyl-binding site formed by Leu285, Leu286, Ser287, and Val288, and oxyanion hole of enzyme formed by Gly116, Gly117, and Ala199. It is observed that the positively charged tertiary amine group of compound **4b** lies between Phe329 and His438 (Fig. 2).

Molecular dynamics simulations

Molecular dynamics simulation is a more useful molecular modeling technique that determines the dynamic behavior of the ligand–protein interactions. In our study, MD simulations were carried out to analyze the stability and hydrogen bonding of compound **4b** in the active site of AChE and BuChE, respectively. Therefore, the calculated best ranking poses of compound **4b** inside AChE (PDB id: 1EVE resolved at 2.5 Å) and the homology model of BuChE using GOLD 5.2.1 program were chosen for molecular dynamics (MD) simulations. These two complexes of compound **4b** and the apo forms of the title proteins were then exposed to 40 ns simulations after the equilibrium step.

Structural stability analysis

On analyzing stability of MD simulations, the RMSD plots of compound **4b** in complex with AChE and BuChE were observed stable during 42 ns, respectively. On the RMSD plot of compound **4b** in complex with AChE, the average RMSD value of complex increases from ~1.0 to ~2.3 Å at the time slot between 0 and 10 ns. It is observed that the average RMSD value slightly decreases to ~2.0 Å after 10 ns and it is to be stable as ~2.0 Å during the rest of MD simulation. The RMSD plot of ligand–protein complex displays forming a stable complex with compound **4b** and protein. On the other hand, the average RMSD value of compound **4b**–BuChE complex gradually increases from ~1.0 to ~3.4 Å at the time slot between 0 and 30 ns on the RMSD plot of compound **4b**–BuChE complex. And then, the average RMSD value is to be stable as ~3.3 Å until at 36 ns. At the rest of MD simulations, the average RMSD value decreases to ~2.5 Å. According to the RMSD plot of compound **4b**–BuChE complex, it is seen that protein forms a stable complex with compound **4b**, however, ligand is flexible in the active site of BuChE due to more fluctuation on the RMSD plot of complex.

When the RMSD plots of the apo forms of both proteins are evaluated, it is specified that the average RMSD value of the apo form of AChE gradually increases from ~1.0 to ~1.7 Å at

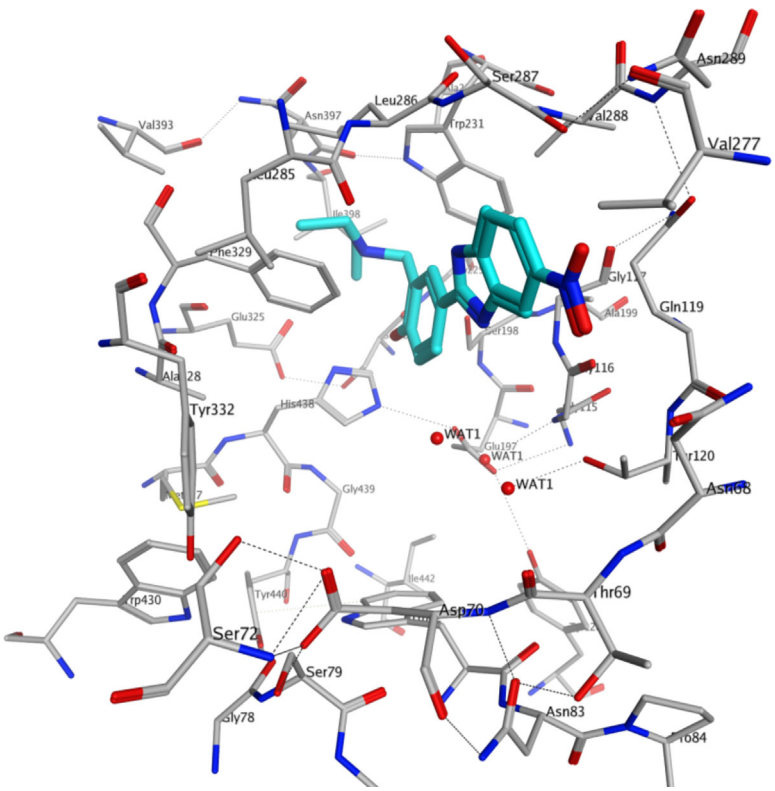

Figure 2. The first ranked solution of compound **4b** using Goldscore in homology model of BuChE. Residues and water molecules are named using three-letter code and specifier. Cyan and white sticks represent compound **4b** and the active site residues, respectively. For clarity, all hydrogen atoms have been removed. H bonds and CH–π interactions are represented black and green dashed lines, respectively.

the time slot between 0 and 15 ns and it keeps stable throughout the rest of MD simulations (Fig. 3). As for the RMSD plot of the apo form of BuChE, the average RMSD value keeps stable as ~1.5 Å throughout the whole MD simulations.

Binding mode analysis

In the current study, it is determined that compound **4b** forms hydrogen bonds with the catalytic site amino acid residues and water molecules and forms water-mediated bridges linking the catalytic site amino acid residues in ligand–AChE complex and hydrogen bonding analysis results were tabulated (Tables 5–8) and MD snapshots were given for displaying hydrogen bonds in Supporting Information Fig. S1. According to analysis results, it is detected three hydrogen bonds are directly formed by ligand with the catalytic site amino acid residues as Tyr121 and Ser122 and Phe330. Besides of directly formed hydrogen bonds, the title compound's heteroatoms form hydrogen bonds with water molecules and form water-mediated bridges linking amino acid residues as Trp84, Tyr121, Ser122, and His440. Nitrogen atoms of imidazole ring bearing hydrogen or not, hydroxyl group of phenol and the positively charged amine group of alkyl chain contribute to forming of hydrogen bonding with water molecules and, water-mediated bridges (Tables 7 and 8). In addition to hydrogen bonding, it is detected that the cation–π, π–π, and H–π interactions are common non-covalent interaction between ligand and protein on binding mode analysis of compound **4b**–AChE complex. The cation–π interaction is specified between the positively charged amine group of alkyl chain of compound **4b** and benzene ring of Tyr334. The average distances between the positively charged nitrogen and carbon atoms of benzene ring of Tyr334 given in Supporting Information Fig. S4 were calculated as 4.78 and 5.10 Å and the distance profile of the cation–π interaction was given as a function of time in Supporting Information Fig. S5. Another interaction which affects binding profile of ligand in the active site of AChE is π–π interaction. This interaction is observed between ligand and amino acid residues as Trp84 and Tyr121. Detected first π–π interaction forms between the benzimidazole core and benzene ring of ligand and the indole ring of Trp84. Second interaction is observed between the benzimidazole core of ligand and benzene ring of Tyr121

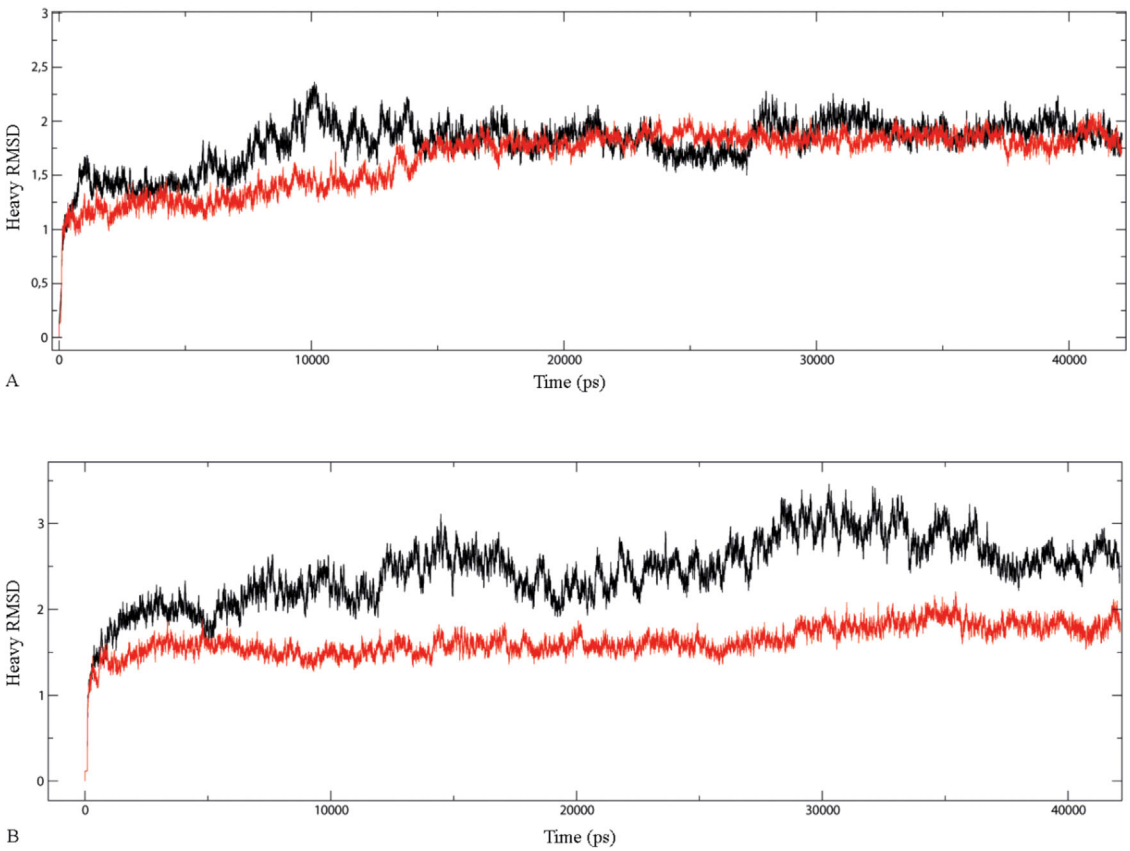

Figure 3. Plots of root-mean square deviation (RMSD) of AChE (PDB id: 1EVE) and AChE–compound **4b** complex (A). Plots of root-mean square deviation (RMSD) of BuChE and BuChE–compound **4b** complex (B). Plots of RMSD of proteins and complexes are represented by red and black, respectively. The trajectories were captured every 1 ps until the simulations end.

Table 5. **The results of hydrogen bonding network between compound 4b and proteins (AChE and BuChE).**

	Acceptor	Donor-H	Donor	H bond occupancy (%)	Distance (Å)	Angle (°)
Compound **4b** (in AchE)	N1	Ser122:HG	Ser122:OG	10.14	2.872	21.61
	Phe330:O	H7	O	4.00	2.703	20.51
	Tyr121:OH	H10	N2	3.44	2.908	16.42
	Leu285:O	H3	N	16.14	2.856	31.09
Compound **4b** (in BuchE)	O2	Asn289:HD21	Asn289:ND2	3.90	2.904	27.93
	O1	Asn289:HD21	Asn289:ND2	3.21	2.902	28.89
	Glu197:O	H7	O	2.69	2.596	17.72

Outputs of hydrogen bonding analysis were obtained by ptraj module of Amber 12. A cutoff of 3.0 Å for distance and 135° for angle were used by ptraj module for hydrogen bonds. The percentage of hydrogen bond was occurring during the process of the MD simulation.

bearing hydroxyl group that forms hydrogen bonds with water molecules as t-shape π–π interaction. H–π interaction is the other factor that contributes ligand binding in this complex. It is observed between *N*,*N*-diethylmethyl group of compound **4b** and benzene rings of Trp84 and Tyr334, and imidazole ring of compound **4b** and hydroxyl group of Ser122, respectively (Supporting Information Fig. S3).

It is considered that hydrogen bonding is an important factor as well as H–π interaction for ligand binding in the compound **4b**–BuChE complex. Hydrogen bonding analysis results of compound **4b**–BuChE complex are shown in Tables 2–5 and MD snapshots are given for displaying hydrogen bonds in Supporting Information Fig. S6. The titled compound forms hydrogen bonds with active site amino acid residues as Glu197, Leu285, and Asn289, and water molecules, and forms water-mediated bridges linking active site amino acid residues which are given in Table 8. Second main interaction for binding of ligand to protein is H–π interaction in ligand–BuChE complex. This interaction is observed between benzimidazole ring of ligand and alkyl side chain of Leu285, the alkyl chains of positively charged amine group of ligand and imidazole ring of His438 (Supporting Information Fig. S6).

Conclusion

A series of Mannich bases of benzimidazole derivatives were synthesized and evaluated for their cholinesterase inhibitory and antioxidant activity. According to the cholinesterase activity results, **4b** and **4c** were the most active compounds against AChE and BuChE, respectively. When all the compounds are evaluated for their antioxidant activity, most of the compounds exhibited close activity to that of tBHQ. These compounds may be considered as important agents for combating oxidative damage in brain. It can be speculated that the Mannich bases of benzimidazole derivatives with phenolic group have multi target potency for AD.

Molecular docking for the synthesis compounds, MD simulations for compound **4b** having highest inhibitor potency against AChE were carried out in the active site of AChE and BuChE, respectively. Docking-guided MD simulations showed that hydrogen bonding networks were found to be crucial for the stability of compound **4b** in the active site of AChE and BuChE, respectively. Forming hydrogen bonds with water molecules and water-mediated bridging were observed more frequent than forming hydrogen bonds with residues inside AChE and BuChE. Apart from

Table 6. **The results of hydrogen bonding network between compound 4b and proteins (AChE and BuChE).**

	Acceptor	Donor-H	Donor	Frames	Frac	Average distance (Å)	Average angle (°)
Compound **4b** (in AChE)	N1	Ser122:HG	Ser122:OG	4271	0.1014	2.8715	158.3856
	Phe330:O	H7	O	1684	0.0400	2.7034	159.4866
	Tyr121:OH	H10	N2	1447	0.0344	2.9082	163.5811
	Leu285:O	H3	N	6797	0.1614	2.8558	148.9134
Compound **4b** (in BuChE)	O2	Asn289:HD21	Asn289:ND2	1644	0.0390	2.9038	152.0746
	O1	Asn289:HD21	Asn289:ND2	1353	0.0321	2.9024	151.1092
	Glu197:OE2	H7	O	1134	0.0269	2.5964	162.2832

Outputs of hydrogen bonding analysis were obtained by cpptraj module of Ambertools 16. A cutoff of 3.0 Å for distance and 135° for angle are used as default criteria by cpptraj module for hydrogen bonds.

Table 7. The results of hydrogen bonding network between compound 4b and water molecules.

	Acceptor	Donor-H	Donor	Count	Frac	Average distance (Å)	Average angle (°)
Compound **4b** (in AChE)	SolventAcc	H7	O	38424	0.9127	2.7174	163.7080
	SolventAcc	H10	N2	24205	0.5749	2.8742	160.5768
	SolventAcc	H3	N	15305	0.3635	2.8876	153.5793
	N1	SolventH	SolventDnr	14693	0.3490	2.8601	159.6981
Compound **4b** (in BuChE)	SolventAcc	H7	O	34675	0.8236	2.7168	160.8984
	SolventAcc	H10	N2	30569	0.7261	2.8562	161.2911
	N1	SolventH	SolventDnr	22687	0.5389	2.8451	159.6121
	SolventAcc	H3	N	11879	0.2822	2.8768	151.8379
	O	SolventH	SolventDnr	8962	0.2129	2.8467	154.8901

Outputs of hydrogen bonding analysis were obtained by cpptraj module of Ambertools 16. A cutoff of 3.0 Å for distance and 135° for angle are used as default criteria by cpptraj module for hydrogen bonds.

hydrogen bonding, cation–π interaction with Tyr334, π–π interaction with Trp84, and t-shape π–π interaction with Tyr121 were found to be important for binding process of compound **4b** inside AChE. Hydrophobic interactions, particularly H–π interactions, were determined important for binding process of compound **4b** as well as hydrogen binding inside BuChE. The analysis of RMSD plots compound **4b** inside proteins displayed that ligand was more flexible inside BuChE compared to AChE.

In summary, these developed Mannich bases of benzimidazole derivatives with phenolic group have potential for further development as a promising lead compounds against AD.

Table 8. The results of hydrogen bonding network between compound 4b and water-mediated bridging residues (in AChE and BuChE).

	Bridging	Residues	Frames
Compound **4b** (in AChE)		Tyr121	9725
		His440	8284
		Trp84	4096
		Ser122	2275
		Glu197	11080
		Asn68	8272
		His438	4251
		Leu286	3912
Compound **4b** (in BuChE)		Ser287	2991
		Gly117	2888
	Gly117	Ser287	2314
		Asp70	1920
		Thr120	1775
	Gln119	Ser287	1379
		Leu285	1298
	Asn68	Asp70	1295

Outputs of hydrogen bonding analysis were obtained by cpptraj module of Ambertools 16. A cutoff of 3.0 Å for distance and 135° for angle are used as default criteria by cpptraj module for hydrogen bonds.

Experimental

Chemistry

General

All melting points were determined with a capillary melting point apparatus (Stuart SMP30, Staffordshire, UK). The IR spectra of the compounds were monitored by attenuated total reflectance (ATR) (PerkinElmer Spectrum 100 FT-IR, Shelton, USA). The NMR spectra (400 MHz for ^{1}H NMR and 100 MHz for ^{13}C NMR) were recorded in the deuterated solvent indicated with chemical shifts reported in d units downfield from tetramethylsilane (TMS). Coupling constants (*J*) are reported in hertz (Hz) (for ^{1}H NMR spectra, AS 400 Mercury Plus NMR Varian, Palo Alto, USA and for ^{13}C NMR spectra, Varian VNMRJ 400). LC/MS was recorded on a Thermo MSQ Plus (San Jose, CA, USA) mass spectrometer using ESI. Analytical thin-layer chromatography (TLC) was run on Merck silica gel plates (Kieselgel 60F254) with detection by UV light (254 nm). All starting materials and reagents were high-grade commercial products.

The InChI codes of the investigated compounds together with some biological activity data are provided as Supporting Information.

General procedure for the synthesis of the Mannich bases

4-(1*H*-Benzimidazole-2-yl)phenol, 4-(5-chloro-1*H*-benzimidazole-2-yl)phenol, 4-(5-methyl-1*H*-benzimidazole-2-yl)phenol, and 4-(5-nitro-1*H*-benzimidazole-2-yl)phenol were synthesized by reacting *o*-phenylenediamine and sodium hydroxy(4-hydroxyphenyl)methane sulfonate salt as described (**1–4**) [24a]. Mannich bases were prepared by a solution of 4-(substituted-benzimidazole)phenol (0.002 mol) in 10 mL ethanol, 0.006 mol of amine derivative and 0.006 mol of formaldehyde. A total of 0.01 mol of trimethylamine was added for alkali pH and then the reaction mixture was refluxed for 30 min. On cooling, the formed product was filtered, dried, and recrystallized.

*4-(1H-Benzo[d]imidazol-2-yl)-2-((dimethylamino)methyl)-phenol (**1a**) [28]*
Beige crystalline (EtOH/H_2O). Yield: 37%; mp 102°C. IR ν_{max} (KBr) cm^{-1}: 3675, 1613, 1593, 1493, 1426, 1271, 1099, 957. LC MS/MS (ES^+) *m/z* 268.17 $[M+1]^{+1}$. ^1H NMR (400 MHz, $CDCl_3$) δ 2.29 (6H, s, H-1‴), 3.61 (2H, s, H-1″), 6.86 (1H, d, *J* = 8.0 Hz, H-6), 7.22 (1H, d, *J* = 3.2 Hz, H-5′/H-6′), 7.23 (1H, d, *J* = 3.2 Hz, H-5′/H-6′), 7.59 (2H, bs, H-4′, H-7′), 7.77 (1H, dd, *J* = 8.0/4.0 Hz, H-5), 7.84 (1H, d, *J* = 2.0 Hz, H-3) ppm. ^{13}C NMR (100 MHz, $CDCl_3$) δ 44.3 (2xC-1‴), 62.3 (C-1″), 116.5 (C-6), 120.6 (C-4), 122.5 (C-5′, C-6′), 122.6 (C-2), 126.9 (C-5), 127.5 (C-3), 152.4 (C-2′), 160.4 (C-1) ppm. Anal. calcd. for $C_{16}H_{17}N_3O$: C, 71.89; H, 6.41; N, 15.72. Found: C, 72.40; H, 6.45; N, 15.29.

*4-(1H-Benzo[d]imidazol-2-yl)-2-((diethylamino)methyl)-phenol (**1b**)*
Light yellow crystalline (EtOH/H_2O). Yield: 17%; mp 190°C. IR ν_{max} (KBr) cm^{-1}: 3674, 3473, 2926, 1609, 1523, 1491, 1472, 1443, 1269, 1092, 1044, 1007, 827, 748. LC MS/MS (ES^+) *m/z* 296.22 $[M+1]^{+1}$. ^1H NMR (400 MHz, $CDCl_3$) δ 1.05 (6H, t, *J* = 7.2 Hz, H-2‴), 2.54 (4H, q, *J* = 7.2 Hz, H-1‴), 3.66 (2H, s, H-1″), 6.81 (1H, d, *J* = 8.4 Hz, H-6), 7.21 (2H, dd, *J* = 6.0/2.8 Hz, H-5′, H-6′), 7.58 (2H, bs, H-4′, H-7′), 7.79 (1H, dd, *J* = 8.4/4.0 Hz, H-5), 7.85 (1H, d, *J* = 2.0 Hz, H-3) ppm. ^{13}C NMR (100 MHz, $CDCl_3$) δ 10.8 (2xC-2‴), 46.0 (2xC-1‴), 56.3 (C-1″), 116.3 (C-6), 120.3 (C-4), 122.2 (C-5′, C-6′), 122.5 (C-2), 126.6 (C-5), 127.3 (C-3), 152.3 (C-2′), 160.5 (C-1) ppm. Anal. calcd. for $C_{18}H_{21}N_3O.0,1H_2O$: C, 72.75; H, 7.19; N, 14.14. Found: C, 73.02; H, 7.15; N, 13.85.

*4-(1H-Benzo[d]imidazol-2-yl)-2-(pyrrolidin-1-ylmethyl)-phenol (**1c**) [28]*
Light brown crystalline (EtOH/H_2O). Yield: 10%; mp 192°C. IR ν_{max} (KBr) cm^{-1}: 3688, 3474, 1609, 1592, 1488, 1402, 1273, 1096, 1007, 820, 738. LC MS/MS (ES^+) *m/z* 294.18 $[M+1]^{+1}$. ^1H NMR (400 MHz, $CDCl_3$) δ 1.86 (4H, s, H-3‴, H-4‴), 2.71 (4H, s, H-2‴, H-5‴), 3.87 (2H, s, H-1″), 6.86 (1H, d, *J* = 8.0 Hz, H-6), 7.22 (2H, dd, *J* = 6.0/3.2 Hz, H-5′, H-6′), 7.60 (2H, dd, *J* = 5.8/3.4 Hz, H-4′, H-7′), 7.77 (1H, d, *J* = 8.0 Hz, H-5), 7.93 (1H, s, H-3) ppm. ^{13}C NMR (100 MHz, $CDCl_3$) δ 23.5 (C-3‴, C-4‴), 53.3 (C-2‴, C-5‴), 57.3 (C-1″), 114.8 (C-4′, C-7′), 116.5 (C-6), 120.3 (C-4), 122.1 (C-2), 122.5 (C-5′, C-6′), 127.4 (C-5), 127.8 (C-3), 138.7 (C-3′a*), 138.9 (C-7′a*), 152.3 (C-2′), 160.3 (C-1) ppm (*, #interchangeable). Anal. calcd. for $C_{18}H_{19}N_3O.2,5H_2O$: C, 63.89; H, 7.15; N, 12.42. Found: C, 63.83; H, 7.01; N, 12.19.

*4-(1H-Benzo[d]imidazol-2-yl)-2-(piperidin-1-ylmethyl)-phenol (**1d**) [28]*
Light beige crystalline (EtOH-H_2O). Yield: 33%; mp 250°C. IR ν_{max} (KBr) cm^{-1}: 3675, 3428, 3023, 2931, 1613, 1522, 1494, 1399, 1274, 1094, 1038, 1009, 822, 743, 735. LC MS/MS (ES^+) *m/z* 308.2 $[M+1]^{+1}$. ^1H NMR (400 MHz, $CDCl_3$) δ 1.55 (2H, m, H-4‴), 1.82 (4H, d, *J* = 1.2 Hz, H-3‴, H-5‴), 2.69 (4H, d, *J* = 1.6 Hz, H-2‴, H-6‴), 4.38 (2H, d, *J* = 4.8 Hz, H-1″), 7.28 (1H, s, H-6), 7.60 (2H, dd, *J* = 6.2/3.1 Hz, H-5′, H-6′), 7.71 (2H, dd, *J* = 6.2/3.0 Hz, H-4′, H-7′), 8.03 (1H, d, *J* = 8.8 Hz, H-5), 8.12 (1H, s, H-3) ppm. ^{13}C NMR (100 MHz, $CDCl_3$) δ 23.8 (C-4‴), 25.7 (C-3‴, C-5‴), 53.7 (C-2‴, C-6‴), 61.6 (C-1″), 116.5 (C-6), 120.6 (C-4), 122.3 (C-2), 122.5 (C-5′, C-6′), 126.9 (C-5), 127.7 (C-3), 152.5 (C-2′), 160.5 (C-1) ppm. Anal. calcd. for $C_{19}H_{21}N_3O$: C, 74.24; H, 6.89; N, 13.67. Found: C, 74.09; H, 7.10; N, 13.11.

*2-[(Dimethylamino)methyl]-4-(5-chloro-1H-benzo[d]-imidazol-2-yl)phenol (**2a**)*
Light pink crystalline (EtAc/*n*-Hex). Yield: 14%; mp 205°C. IR ν_{max} (KBr) cm^{-1}: 3594, 3430, 3057, 2946, 2920, 1445, 844, 711, 518. LS MS/MS (ES^+) *m/z* 302.21 $[M+1]^{+1}$, 304.16 [M+2]. ^1H NMR (400 MHz, $CDCl_3$) δ 2.26 (6H, s, H-1‴), 3.55 (2H, s, H-1″), 6.84 (1H, d, *J* = 8.4 Hz, H-6), 7.22 (1H, dd, *J* = 8.6/1.8 Hz, H-6′), 7.46 (1H, bs, H-4′/H-7′), 7.52 (1H, bs, H-4′/H-7′), 7.77 (1H, dd, *J* = 8.4/2.4 Hz, H-5), 7.79 (1H, d, *J* = 2.0 Hz, H-3) ppm. ^{13}C NMR (100 MHz, $CDCl_3$) δ 44.3 (2xC-1‴), 62.3 (C-1″), 116.6 (C-6), 120.0 (C-4), 122.7 (C-2*), 123.1 (C-6′*), 127.0 (C-5), 127.5 (C-3), 128.1 (C-5′), 153.5 (C-2′), 160.8 (C-1) ppm. Anal. calcd. for $C_{16}H_{16}ClN_3O$: C, 63.68; H, 5.34; N, 13.92. Found: C, 63.99; H, 5.68; N, 13.86.

*2-[(Diethylamino)methyl]-4-(5-chloro-1H-benzo[d]-imidazol-2-yl)phenol (**2b**)*
Light violet crystalline (EtAc/*n*-Hex). Yield: 12%; mp 150°C. IR ν_{max} (KBr) cm^{-1}: 3594, 3242, 3082, 2948, 1558, 1535, 995, 742, 526. LC MS/MS (ES^+) *m/z* 330.23 $[M+1]^{+1}$, 332.21 [M+2]. ^1H NMR (400 MHz, $CDCl_3$) δ 1.13 (6H, t, *J* = 7.0 Hz, H-2‴), 2.67 (4H, q, *J* = 7.2 Hz, H-1‴), 3.84 (2H, s, H-1″), 6.85 (1H, d, *J* = 8.4 Hz, H-6), 7.18 (1H, dd, *J* = 8.4/1.6 Hz, H-6′), 7.49 (1H, bs, H-4′/H-7′), 7.56 (1H, bs, H-4′/H-7′), 7.70 (1H, d, *J* = 8.0 Hz, H-5), 7.85 (1H, s, H-3) ppm. ^{13}C NMR (100 MHz, $CDCl_3$) δ 10.9 (2xC-2‴), 46.3 (2xC-1‴), 56.2 (C-1″), 116.7 (C-6), 120.0 (C-4), 122.4 (C-2), 123.0 (C-6′), 127.2 (C-5), 127.8 (C-3), 128.0 (C-5′), 153.6 (C-2′), 161.0 (C-1) ppm. Anal. calcd. for $C_{18}H_{20}ClN_3O.H_2O$: C, 62.15; H, 6.37; N, 12.08. Found: C, 62.36; H, 6.03; N, 12.48.

*4-(5-Chloro-1H-benzo[d]imidazol-2-yl)-2-(pyrrolidin-1-ylmethyl)phenol (**2c**)*
Light violet crystalline (EtAc/*n*-Hex). Yield: 12%; mp 163°C. IR ν_{max} (KBr) cm^{-1}: 3588, 3242, 3113, 2947, 1558, 1492, 1445, 1271, 998, 844, 735, 519. LC MS/MS (ES^+) *m/z* 328.17 $[M+1]^{+1}$, 330.21 [M+2]. ^1H NMR (400 MHz, $CDCl_3$) δ 1.88 (4H, s, H-3‴, H-4‴), 2.68 (4H, s, H-2‴, H-5‴), 3.92 (2H, s, H-1″), 6.91 (1H, d, *J* = 8.8 Hz, H-6), 7.20 (1H, dd, *J* = 8.4/1.6 Hz, H-6′), 7.52 (1H, s, H-4′/H-7′), 7.68 (1H, dd, *J* = 8.6/2.2 Hz, H-5), 7.83 (1H, s, H-3) ppm. ^{13}C NMR (100 MHz, $CDCl_3$) δ 23.5 (C-3‴, C-4‴), 53.4 (C-2‴, C-5‴), 57.9 (C-1″), 116.5 (C-6), 120.1 (C-4), 122.9 (C-2*), 123.0 (C-6′*), 127.1 (C-5), 127.4 (C-3), 128.4 (C-5′), 153.2 (C-2′), 160.8 (C-1) ppm. Anal. calcd. for $C_{18}H_{18}ClN_3O$: C, 65.95; H, 5.53; N, 12.82. Found: C, 65.90; H, 5.39; N, 12.38.

*4-(5-Chloro-1H-benzo[d]imidazol-2-yl)-2-(piperidin-1-ylmethyl)phenol (**2d**)*
Beige crystalline (EtAc/*n*-Hex). Yield: 29%; mp 166°C. IR ν_{max} (KBr) cm^{-1}: 3596, 3232, 2845, 1593, 1488, 1443, 998, 843, 551.

LC MS/MS (ES^+) *m/z* 342.21 $[M+1]^{+1}$, 344.16 [M+2]. ^1H NMR (400 MHz, $CDCl_3$) δ 0.88 (2H, m, H-4‴), 1.25 (4H, s, H-3‴, H-5‴), 1.70 (4H, m, H-2‴, H-6‴), 3.81 (2H, s, H-1″), 6.87 (1H, d, $J = 8.4$ Hz, H-6), 7.19 (1H, dd, $J = 8.4/2.0$ Hz, H-6′), 7.50 (1H, d, $J = 8.4$ Hz, H-7′), 7.57 (1H, s, H-4′), 7.72 (1H, dd, $J = 8.4/2.0$ Hz, H-5), 7.93 (1H, s, H-3) ppm. ^{13}C NMR (100 MHz, $CDCl_3$) δ 23.6 (C-4‴), 25.4 (C-3‴, C-5‴), 53.6 (C-2‴, C-6‴), 61.1 (C-1″), 116.6 (C-6), 120.0 (C-4), 121.9 (C-2), 123.0 (C-6′), 127.3 (C-5), 127.9 (C-3), 128.0 (C-5′), 153.5 (C-2′), 160.8 (C-1) ppm. Anal. calcd. for $C_{19}H_{20}ClN_3O$: C, 66.76; H, 5.90; N, 12.29. Found: C, 66.96; H, 6.05; N, 12.70.

*2-[(Dimethylamino)methyl]-4-(5-methyl-1H-benzo[d]-imidazol-2-yl)phenol (**3a**)*
Light brown crystalline (MeOH/H_2O). Yield: 60%; mp 125°C. IR ν_{max} (KBr) cm^{-1}: 3576, 3256, 2930, 1610, 1524, 1446, 1274, 1098, 1019, 985, 896, 824, 802, 737. LC MS/MS (ES^+) *m/z* 282.19 $[M+1]^{+1}$. ^1H NMR (400 MHz, $CDCl_3$) δ 2.29 (6H, s, H-1‴), 2.46 (3H, s, Ar-CH_3), 3.61 (2H, s, H-1″), 6.86 (1H, d, $J = 8.4$ Hz, H-6), 7.05 (1H, dd, $J = 8.6/1.4$ Hz, H-6′), 7.36 (1H, s, H-4′/H-7′), 7.49 (1H, s, H-4′/H-7′), 7.73 (1H, dd, $J = 8.6/2.2$ Hz, H-5), 7.82 (1H, d, $J = 2.4$ Hz, H-3) ppm. ^{13}C NMR (100 MHz, $CDCl_3$) δ 21.6 (Ar-CH_3), 44.2 (2xC-1‴), 62.2 (C-1″), 114.2 (C-4′*), 114.8 (C-7′*), 116.5 (C-6), 120.6 (C-4), 122.5 (C-2), 124.0 (C-6′), 127.0 (C-5), 127.5 (C-3), 132.4 (C-5′), 137.5 (C-3′a#), 138.7 (C-7′a#), 152.1 (C-2′), 160.3 (C-1) ppm. Anal. calcd. for $C_{17}H_{19}N_3O.0{,}8CH_3OH$: C, 69.64; H, 7.29; N, 13.69. Found: C, 69.41; H, 6.91; N, 13.72.

*2-[(Diethylamino)methyl]-4-(5-methyl-1H-benzo[d]-imidazol-2-yl)phenol (**3b**)*
Light yellow crystalline (EtOH/H_2O). Yield: 26%; mp 135°C. IR ν_{max} (KBr) cm^{-1}: 3689, 3372, 2973, 1608, 1444, 1272, 1055, 800, 738. LC MS/MS (ES^+) *m/z* 310.21 $[M+1]^{+1}$. ^1H NMR (400 MHz, $CDCl_3$) δ 1.08 (6H, t, $J = 7.2$ Hz, H-2‴), 2.45 (3H, s, Ar-CH_3), 2.59 (4H, q, $J = 7.2$ Hz, H-1‴), 3.74 (2H, s, H-1″), 6.83 (1H, d, $J = 8.8$ Hz, H-6), 7.04 (1H, d, $J = 8.4$ Hz, H-6′), 7.35 (1H, s, H-4′), 7.48 (1H, d, $J = 8.0$ Hz, H-7′), 7.61 (1H, d, $J = 8.2$ Hz, H-5), 7.82 (1H, s, H-3) ppm. ^{13}C NMR (100 MHz, $CDCl_3$) δ 11.0 (2xC-2‴), 21.6 (Ar-CH_3), 46.2 (2xC-1‴), 56.4 (C-1″), 116.5 (C-6), 120.4 (C-4), 122.5 (C-2), 123.9 (C-6′), 126.8 (C-5), 127.4 (C-3), 132.3 (C-5′), 152.3 (C-2′), 160.6 (C-1) ppm. Anal. calcd. for: $C_{19}H_{23}N_3O.2H_2O$: C, 66.06; H, 7.88; N, 12.16. Found: C, 66.42; H, 7.46; N, 12.41.

*4-(5-Methyl-1H-benzo[d]imidazol-2-yl)-2-(pyrrolidin-1-ylmethyl)phenol (**3c**)*
Off-white crystalline (EtOH/H_2O). Yield: 10%; mp 176°C. IR ν_{max} (KBr) cm^{-1}: 3675, 3452, 1558, 1278, 1098, 864, 846, 808. LC MS/MS (ES^+) *m/z* 308.27 $[M+1]^{+1}$. ^1H NMR (400 MHz, $CDCl_3$) δ 1.77 (4H, s, H-3‴, H-4‴), 2.38 (3H, s, Ar-CH_3), 2.58 (4H, s, H-2‴, H-5‴), 3.72 (2H, s, H-1″), 6.76 (1H, d, $J = 8.0$ Hz, H-6), 6.98 (1H, d, $J = 8.0$ Hz, H-6′), 7.33 (1H, s, H-4′), 7.45 (1H, d, $J = 8.0$ Hz,H-7′), 7.82 (1H, d, $J = 7.6$ Hz, H-5), 7.90 (1H, s, H-3) ppm. ^{13}C NMR (100 MHz, $CDCl_3$) δ 21.6 (Ar-CH_3), 23.5 (C-3‴, C-4‴), 53.7 (C-2‴, C-5‴), 56.1 (C-1″), 115.1 (C-6), 120.3 (C-4), 123.6(C-2), 124.1 (C-6′), 126.8 (C-5), 128.9 (C-3), 132.0 (C-5′), 152.5(C-2′), 158.5 (C-1) ppm. Anal. calcd. for $C_{19}H_{21}N_3O.2H_2O$: C, 66.45; H, 7.34; N, 12.24. Found: C, 66.92; H, 7.11; N, 12.51.

*4-(5-Methyl-1H-benzo[d]imidazol-2-yl)-2-(piperidin-1-ylmethyl)phenol (**3d**)*
Light brown crystalline (EtAc/*n*-Hex). Yield: 37%; mp 165°C. IR ν_{max} (KBr) cm^{-1}: 3570, 3443, 3032, 2975, 1429, 1276, 1098, 907, 810, 737. LC MS/MS (ES^+) *m/z* 322.19 $[M+1]^{+1}$. ^1H NMR (400 MHz, $CDCl_3$) 1.46 (2H, s, H-4‴), 1.59 (4H, t, $J = 5.2$ Hz, H-3‴, H-5‴), 2.43 (7H, s, Ar-CH_3, H-2‴, H-6‴), 3.56 (2H, s, H-1″), 6.80 (1H, d, $J = 8.4$ Hz, H-6), 7.03 (1H, dd, $J = 8.0/0.8$ Hz, H-6′), 7.34 (1H, s, H-4′), 7.47 (1H, d, $J = 8.4$ Hz, H-7′), 7.77 (1H, dd, $J = 8.4/2.0$ Hz, H-5), 7.81 (1H, s, H-3) ppm. ^{13}C NMR (100 MHz, $CDCl_3$) δ 21.6 (Ar-CH_3), 23.7 (C-4‴), 25.6 (C-3‴, C-5‴), 53.6 (C-2‴, C-6‴), 61.5 (C-1″), 114.3 (C-4′*), 114.7 (C-7′*), 116.4 (C-6), 120.5 (C-4), 122.1 (C-2), 124.0 (C-6′), 126.9 (C-5), 127.7 (C-3), 132.3 (C-5′), 152.2 (C-2′), 160.3 (C-1) ppm. Anal. calcd. for $C_{20}H_{23}N_3O.0{,}4C_4H_8O_2$: C, 72.74; H, 7.40; N, 11.78. Found: C, 72.96; H, 7.40; N, 11.53.

*4-(5-Nitro-1H-benzo[d]imidazol-2-yl)phenol (**4**)*
Yellow crystalline (MetOH/H_2O). Yield: 52%; mp >300°C. IR ν_{max} (KBr) cm^{-1}: 3439, 3292, 2918, 1612, 1505, 1445, 1329, 1283, 1176, 1067, 838, 734. LC MS/MS (ES^+) *m/z* 256.13 $[M+1]^{+1}$. H NMR (400 MHz, CD_3OD) δ 6.95 (2H, d, $J = 8.6$ Hz, H-2, H-6), 7.64 (1H, d, $J = 8.6$ Hz, H-7′), 7.97 (2H, d, $J = 9.0$ Hz, H-3, H-5), 8.15 (1H, dd, $J = 8.8/2.0$ Hz, H-6′) 8.43 (1H, d, $J = 1.6$ Hz, H-4′) ppm. ^{13}C NMR (100 MHz, CD_3OD) δ 115.9 (C-2, C-6), 118.1 (C-6′), 119.9 (C-4), 128.9 (C-3, C-5), 143.6 (C-2′), 160.8 (C-1) ppm. Anal. calcd. for $C_{13}H_9N_3O_3$: C, 61.18; H, 3.55; N, 16.46. Found: C, 61.58; H, 3.78; N, 16.20.

*2-[(Dimethylamino)methyl]-4-(5-nitro-1H-benzo[d]-imidazol-2-yl)phenol (**4a**)*
Yellow crystalline (EtAc/*n*-Hex). Yield: 37%; mp 135°C. IR ν_{max} (KBr) cm^{-1}: 3592, 3421, 1600, 1490, 1336, 1014, 834. LC MS/MS (ES^+) *m/z* 313.14 $[M+1]^{+1}$. ^1H NMR (400 MHz, DMSO-d_6) δ 2.27 (6H, s, H-1‴), 3.66 (2H, s, H-1″), 6.91 (1H, d, $J = 8.4$ Hz, H-6), 7.67 (1H, d, $J = 8.8$ Hz, H-7′), 7.96 (1H, dd, $J = 8.4/2.0$ Hz, H-6′), 7.98 (1H, s, H-4′), 8.07 (1H, dd, $J = 8.8/2.0$ Hz, H-5), 8.38 (1H, d, $J = 2.0$ Hz, H-3) ppm. ^{13}C NMR (100 MHz, $CDCl_3$) δ 44.4 (2xC-1‴), 62.4 (C-1″), 116.8 (C-6), 118.7 (C-4*), 119.3 (C-6′*), 123.0 (C-2), 127.2 (C-5), 127.8 (C-3), 143.6 (C-5′), 161.7 (C-1) ppm. Anal. calcd. for $C_{15}H_{14}N_4O_3.2C_4H_8O_2$: C, 58.22; H, 6.37; N, 11.81. Found: C, 58.42; H, 6.42; N, 11.64.

*2-[(Diethylamino)methyl]-4-(5-nitro-1H-benzo[d]-imidazol-2-yl)phenol (**4b**)*
Yellow crystalline (EtAc/*n*-Hex). Yield: 12%; mp 116°C. IR ν_{max} (KBr) cm^{-1}: 3587, 3058, 1682, 1609, 1337, 1273, 998, 738, 717. LC MS/MS (ES^+) *m/z* 341.16 $[M+1]^{+1}$. ^1H NMR (400 MHz, DMSO-d_6) δ 1.05 (6H, t, $J = 7.2$ Hz, H-2‴), 2.60 (4H, q, $J = 7.2$ Hz, H-1‴), 3.8 (2H, s, H-1″), 6.87 (1H, d, $J = 8.0$ Hz, H-6), 7.67 (1H, d, $J = 7.6$ Hz, H-6′), 7.95 (1H, d, $J = 8.4$ Hz, H-7′), 7.96 (1H, s, H-4′),

8.07 (1H, dd, $J = 8.8/2.4$, Hz, H-5), 8.37 (1H, s, H-3) ppm. ^{13}C NMR (100 MHz, $CDCl_3$) δ 11.0 (2xC-2‴), 46.3 (2xC-1‴), 56.5 (C-1″), 116.9 (C-6), 118.6 (C-4*), 119.3 (C-6′*), 122.9 (C-2), 127.3 (C-5), 127.8 (C-3), 143.5 (C-2′), 162.2 (C-1) ppm. Anal. calcd. for $C_{17}H_{18}N_4O_3.C_4H_8O_2$: C, 60.86; H, 6.32; N, 13.52. Found: C, 61.38; H, 6.25; N, 13.92.

*4-(5-Nitro-1H-benzo[d]imidazol-2-yl)-2-(pyrrolidin-1-ylmethyl)phenol (**4c**)*

Orange crystalline (MeOH/H_2O). Yield: 34%; mp 140°C. IR ν_{max} (KBr) cm^{-1}: 3598, 3448, 1685, 1508, 1490, 1424, 1417, 1270, 851, 720. LC MS/MS (ES^+) *m/z* 339.08 $[M+1]^{+1}$. ^{1}H NMR (400 MHz, DMSO-d_6) δ 1.82 (4H, s, H-3‴, H-4‴), 2.79 (4H, s, H-2‴, H-5‴), 3.98 (2H, s, H-1″), 6.97 (1H, d, $J = 8.4$ Hz, H-6), 7.68 (1H, d, $J = 6.4$ Hz, H-6′), 7.99 (1H, d, $J = 9.6$ Hz, H-7′), 8.07 (1H, d, $J = 1.6$ Hz, H-4′), 8.09 (1H, s, H-5), 8.38 (1H, s, H-3) ppm. ^{13}C NMR (100 MHz, $CDCl_3$) δ 23.6 (C-3‴, C-4‴), 53.4 (C-2‴, C-5‴), 58.2 (C-1″), 116.8 (C-6), 118.5 (C-4*), 119.1 (C-6′*), 123.0 (C-2), 127.6 (C-3′a#), 127.7 (C-5#), 143.3 (C-5′), 156.7 (C-2′), 161.7 (C-1) ppm. Anal. calcd. for $C_{18}H_{18}N_4O_3.H_2O$: C, 60.66; H, 5.66; N, 15.72. Found: C, 59.94; H, 5.55; N, 15.86.

*4-(5-Nitro-1H-benzo[d]imidazol-2-yl)-2-(piperidin-1-ylmethyl)phenol (**4d**)*

Orange crystalline (EtAc/*n*-Hex). Yield: 6%; mp 109°C. IR ν_{max} (KBr) cm^{-1}: 3588, 3426, 1686, 1558, 1506, 1492, 1272, 997, 814, 734. LC MS/MS (ES^+) *m/z* 353.16 $[M+1]^{+1}$. ^{1}H NMR (400 MHz, $CDCl_3$) δ 1.51 (2H, s, H-4‴), 1.64 (4H, s, H-3‴, H-5‴), 2.51 (4H, s, H-2‴, H-6‴), 3.72 (2H, s, H-1″), 6.89 (1H, d, $J = 8.4$ Hz, H-6), 7.60 (1H, d, $J = 8.8$ Hz, H-6′), 7.80 (1H, d, $J = 7.8$ Hz, H-7′), 7.86 (1H, s, H-4′), 8.17 (1H, dd, $J = 8.8/2.0$ Hz, H-5), 8.46 (1H, s, H-3) ppm. ^{13}C NMR (100 MHz, $CDCl_3$) δ 23.8 (C-4‴), 25.7 (C-3‴, C-5‴), 53.8 (C-2‴, C-6‴), 61.9 (C-1″), 116.8 (C-6), 118.6 (C-4*), 119.2 (C-6′*),122.6 (C-2), 127.1 (C-5), 128.0 (C-3), 143.6 (C-5′), 161.7 (C-1) ppm. Anal. calcd. for $C_{18}H_{18}N_4O_3.C_4H_8O_2$: C, 62.71; H, 6.41; N, 12.72. Found: C, 62.40; H, 6.48; N, 12.40.

Biological activity assays

Inhibition of AChE/BuChE

AChE (E.C.3.1.1.7., Type VI-S, from electric eel) and BuChE (E.C. 3.1.1.8, from equine serum) were purchased from Sigma–Aldrich (Steinheim, Germany). 5,5-Dithiobis(2-nitrobenzoic acid) (DTNB, Ellman's reagent), buffer compounds (potassium dihydrogen phosphate, potassium hydroxide), sodium hydrogen carbonate and acetylthiocholine iodide (ATC), butyrylthiocholine iodide (BTC) used as substrates were obtained from Fluka (Buchs, Switzerland). Spectrophotometric measurements were performed on a Shimadzu UV/160-A spectrophotometer.

AChE/BuChE enzyme activities were investigated using a slightly modified colorimetric method of Ellman et al. [32]. As the product of the enzymatic hydrolysis, the thiocholine does not possess a significant chromophore for UV detection; the evaluation of enzyme activity was performed using a specific chromogenic reagent, DTNB. Stock solutions of the inhibitor compounds were prepared in 2% dimethylsulfoxide (DMSO), which were diluted with aqueous assay medium to a final content of organic solvent always lower than 0.2%. The enzyme activity was determined in the presence of at least five different concentrations of an inhibitor, generally between 10^{-3} and 10^{-8}, in order to obtain the inhibition of AChE or BuChE activity between 0 and 100%. Each concentration was assayed in triplicate. Prior to use, all solutions were adjusted to 20°C. Enzyme solution (2.5 units/mL, 100 μL) and inhibitor solution (100 μL) were added into a cuvette containing the phosphate buffer (3.0 mL, 0.1 M; pH 8.0). After 5 min of incubation, required aliquots of the DTNB solution (0.01 M, 100 mL) and of the ATC/BTC (0.075 M, 20 μL) were added. After a rapid and immediate mixing, the absorption was measured at 412 nm.

Brain supernatant preparation

Adult Sprague-Dawley rats weighing 180–240 g were used for the current study. All animals were maintained on a 12:12 h dark–light cycle, with free access to chow and water. The protocol for the experiment was approved by the Appropriate Animal Care Committee of Ege University. All efforts were made to minimize the number of animals used and their suffering. On the day of the experiment, the rats were decapitated and whole brain samples dissected on ice. The sample of brain tissue was weighed and homogenized (1:10, w/v) in 20 mM phosphate buffer (pH 7.4) containing 140 mM potassium chloride at +4°C. The homogenate was centrifuged at 1200×*g* for 10 min at +4°C. The supernatant was separated and incubated at 37°C for 60 min in the presence of Fe^{2+}/ascorbic acid and/or synthesized compounds (10^{-4}, 10^{-5}, and 10^{-6} M) or tBHQ (50 μM) as an antioxidant agent. A total of 0.2 mL supernatant obtained from brain tissue was incubated at 37°C for 60 min in the presence of 0.04 mL of Tris-HCl (pH 7.2), 0.02 mL of 0.1 mM ascorbic acid, 0.02 mL of 4 mM $FeCl_2$, and 0.02 mL of 0.1 mM concentrations of synthesized compounds according to the procedure previously described by Olgen et al. [35]. Immediately, aliquots were taken to measure lipid peroxidation (thiobarbituric acid reactive species, TBARS) and ROS production. We carried out parallel experiments with various blanks in the presence or absence of Fe^{2+} and ascorbic acid or compounds. The protein content of the supernatant was measured by using bovine-serum albumin as a standard, as described by the method of Lowry et al. [36].

Assay of lipid peroxidation

TBARS were estimated by the double heating method of Draper and Hadley [37]. The principle of the method is the spectrophotometric measurement of the color generated by the reaction of thiobarbituric acid (TBA) with malondialdehyde (MDA). Briefly, 2.5 mL of 10% trichloroacetic acid (TCA) solution was added to 0.5 mL of aliquots from the incubation medium in each centrifuge tube and the tubes were placed in a boiling water bath for 15 min. After cooling in tap water, the tubes were centrifuged at 1000×*g* for 10 min, and 2 mL of

the supernatant was added to 1 mL of 0.67% TBA solution in a test tube and the tube was placed in a boiling water bath for 15 min. The solution was then cooled in tap water and its absorbance was measured at 532 nm. The concentration of MDA was calculated by using 1,1,3,3-tetramethoxypropane as a standard. The levels of MDA were expressed as nmol MDA/mg protein and represented as a percentage of the control.

Measurement of ROS production

Reactive oxygen species formation was measured in brain supernatants, according to a previous report [38]. Briefly, supernatants were diluted in nine volumes of 40 mM Tris + HEPES buffer and incubated with 5 μM 2′,7′-dichlorofluorescein diacetate (DCF-DA) reagent at 37°C for 30 min in the presence of $FeCl_2$/ascorbate or in the presence of phenolic Mannich bases of benzimidazole derivatives (10^{-4}, 10^{-5}, and 10^{-6} M). At the end of incubation, fluorescent signals were recorded at excitation and emission wavelengths of 488 and 532 nm, respectively. Results were expressed as percentage of the control.

Molecular docking study

Homology modeling

Sequences of *Equus caballus* (horse) BuChE (Q9N1N9) was obtained from The Universal Protein Resource Knowledgebase (UniProtKB). Homology model of *eq*BuChE was generated using SWISS-MODEL server [39, 40]. For this purpose, the crystal structure of *hu*BuChE (PDB id: 4TPK resolved at 2.7 Å) displaying a primary amino acid sequence identity of 90.80% with *eq*BuChE was selected as a template structure for building homology model. After the model was constructed, the crude model was aligned with chain A of the crystal structure of *hu*BuChE (PDB id: 4TPK) for determining the binding site residues of the model. The crude model was prepared using xleap module of AmberTools 16 with AMBER99SB force field and solvated in an octahedral box with TIP3P water molecules with 10 Å distance between the protein surface and the box boundary [41, 42]. Then the solvated model was neutralized with appropriate number of chlorine counter ions and exposed to an energy minimization with Sander.MPI modul of Amber 12 suite [43].

Ligand docking

The chemical structures of titled compounds were created with builder panel of MOE2015.10, protonated using the protonate 3D protocol and exposed to an energy minimization with MOE.2015.10 using MMFF94x force field [44, 45]. The crystal structure of AChE (PDB id: 1EVE resolved at 2.5 Å) was obtained from the RCSB Protein Data Bank (http://www.rcsb.org/pdb). Chain A was selected for docking structure and chain B, heteroatoms, water molecules in the pdb file were removed. Chain A was prepared using xleap module of AmberTools 16 with AMBER99SB force field and solvated in an octahedral box with TIP3P water molecules with 10 Å distance between the protein surface and the box boundary [42]. Then the solvated chain of AChE was neutralized with appropriate number of sodium counter ions and exposed to an energy minimization with Sander.MPI modul of Amber 12 suite. After the energy minimization, generated sodium counter ions and water molecules (excluded the water molecules included in the binding site) were deleted from system for using docking study.

Homology model of BuChE was prepared for docking procedure removing water molecules apart from the water molecules included in the binding site and chlorine counter ions generated by xleap module of AmberTools 16. Docking of the ligands was carried out using GOLD 5.2.1 program with default generic algorithm parameters [46, 47]. The studied compounds were docked within a radius of 22 Å around the nitrogen atom (N1) of the imidazole group of His440 existed the binding site of AchE and His438 existed the binding site of the homology model of BuChE. Hundred conformations were allowed per structure. GoldScore fitness function is used as scoring functions [46, 47]. Figures 1 and 2 were created with MOE2015.10 program.

Molecular dynamics simulations

Molecular dynamics simulations were performed for apo form of proteins (AChE and BuChE) and protein–ligand complexes using AMBER12 [43]. The initial protein–ligand complexes were prepared using first ranked docking poses of compound **4b** in AChE and BuChE obtained from docking studies. Antechamber module of AmberTools 16 was used to calculate the partial atomic charges for compound **4b** with AM1-BCC charge model [43, 48]. The apo form and complex systems were prepared for the energy minimizations and MD simulations using xleap module of AmberTools 16 [43]. General AMBER force field (gaff) for ligand and AMBERff99SB force field for proteins were exploited to parameterize the systems [41, 49]. Apo form of AChE and ligand–AChE complex were neutralized with appropriate number of sodium counter ions and apo form of BuChE and ligand–BuChE complex were neutralized with appropriate number of chlorine counter ions. The whole systems were solvated in an octahedral box with TIP3P water molecules with 10 Å distance between the protein surface and the box boundary [42]. SANDER.MPI and PMEMD.CUDA modules of AMBER12 were used to realize the energy minimizations and MD simulations of the systems, respectively [43]. In order to avoid bad steric contacts, the initial systems were exposed to energy minimization in two steps. In the first step, energy minimizations were utilized restraining initial structures for 1000 iterations with steepest descent algorithm and for 1000 iterations with conjugate gradient methods. At last step, whole systems were subjected to energy minimization for 2500 iterations using steepest descent algorithm and for 2500 iterations using conjugate gradient methods. In the heating step (0.1 ns), the systems were heated from 0 to 300 K with 10 kcal/mol/Å restraint force permitting water molecules and ions to move freely. In the equilibration step (2 ns), Langevin dynamics were used to equilibrate the temperature at 300 K with the collision frequency of 1.0 ps^{-1} in constant volume periodic boundary

for the entire systems. After the temperature stabilized at 300 K, the pressure was equilibrated at 1 bar with keeping positional restrains for the solute using constant pressure periodic boundary conditions with isotropic position scaling method. In the free MD simulation, the positional constrains were gradually removed keeping the temperature at 300 K and pressure at 1 bar. In the equilibration and the free MD steps, the SHAKE algorithm was carried out in order to constrain band vibrations involving hydrogen atoms [50]. The Particle Mesh Ewald (PME) method was performed for long-range electrostatic interactions using 10 Å cutoff for the short-range non-bonded interactions and 2 fs for a time step [51]. The whole systems were exposed to free MD simulation for 40 ns. Xmgrace program was used for visualization of the trajectories [52]. The hydrogen bonding was detected with *Cpptraj* module of AmberTools 16 using default parameters and *ptraj* module of AMBER 12 package using the maximum donor–acceptor distance of 3.0 Å and a donor-hydrogen-acceptor angle of 135° [53, 54]. MD snapshots were extracted from free MD simulations using UCSF Chimera package [55]. Figures were set up with MOE2015.10 program.

LogP and SLogP predictions

LogP and SLogP values of the compounds were calculated using MOE2015.10 [56].

This study was supported by research grants from Ege University (Project Number: 12/ECZ/022). The authors would like to thank the Pharmaceutical Sciences Research Centre (FABAL) at Ege University Faculty of Pharmacy for spectral analyses of the compounds and molecular modeling software support.

The authors have declared no conflicts of interest.

References

[1] D. M. Walsh, D. J. Selkoe, *Neuron* **2004**, *44*, 181–193.
[2] R. Brookmeyer, E. Johnson, K. Ziegler-Graham, H. M. Arrighi, *Alzheimer's Dement*. **2007**, *3*, 186–191.
[3] E. K. Perry, B. E. Tomlinson, G. Blesseed, K. Bergmann, P. H. Gibson, R. H. Perry, *Br. Med. J.* **1978**, *2*, 1457–1459.
[4] L. Savini, A. Gaeta, C. Fattorusso, B. Catalanotti, G. Campiani, L. Chiasserini, C. Pellerano, E. Novellino, D. McKissic, A. Saxena, *J. Med. Chem*. **2003**, *46*, 1–4.
[5] M. F. Eskander, N. G. Nagykery, E. Y. Leung, B. Khelghati, C. Geula, *Brain Res*. **2005**, *1060*, 144–152.
[6] E. Giacobini, in *Cholinesterases and Cholinesterase Inhibitors* (Ed.: E. Giacobini), Martin Dunitz Ltd., London **2000**, pp. 181–226.
[7] M. Mesulam, A. Guillozet, P. Shaw, B. Quinn, *Neurobiol. Dis*. **2002**, *9*, 88–93.
[8] M. I. Fernández-Bachiller, C. Pérez, L. Monjas, J. Rademann, M. I. Rodríguez-Franco, *J. Med. Chem*. **2012**, *55*, 1303–1317.
[9] S. Varadarajan, S. Yatin, M. Aksenova, D. A. Butterfield, *J. Struct. Biol*. **2000**, *130*, 184–208.
[10] X. Wang, W. Wang, L. Li, G. Perry, H. Lee, X. Zhu, *Biochim. Biophys. Acta* **2014**, *1842*, 1240–1247.
[11] F. Gu, M. Zhu, J. Shi, Y. Hu, Z. Zhao, *Neurosci. Lett*. **2008**, *440*, 44–48.
[12] J. S. Lan, S. S. Xie, S. Y. Li, L. F. Pan, X. B. Wang, L. Y. Kong, *Bioorg. Med. Chem*. **2014**, *22*, 6089–6104.
[13] C. M. Lauderback, J. M. Hackett, J. N. Keller, S. Varadarajan, L. Szweda, M. Kindy, W. R. Markesbery, D. A. Butterfield, *Biochemistry* **2001**, *40*, 2548–2554.
[14] Y. Bansal, O. Silakari, *Bioorg. Med. Chem*. **2012**, *20*, 6208–6236.
[15] A. Mavrova, D. Yancheva, N. Anastassova, K. Anichina, J. Zvezdanovic, A. Djordjevic, D. Markovic, A. Smelcerovic, *Bioorg. Med. Chem*. **2015**, *23*, 6317–6326.
[16] D. Song, S. Ma, *ChemMedChem* **2016**, *11*, 646–659.
[17] K. Błaszczak-Świątkiewicz, P. Olszewska, E. Mikiciuk-Olasik, *Pharmacol. Rep*. **2014**, *66*, 100–106.
[18] Y. Ozkay, Y. Tunai, H. Karaca, I. Isikdag, *Eur. J. Med. Chem*. **2010**, *45*, 3293–3298.
[19] L. B. Townsend, D. S. Wise, *Trends. Parasitol*. **1990**, *6*, 107–112.
[20] J. R. Kumar, J. Jawaharand, D. P. Pathak, *E-J. Chem*. **2006**, *3*, 278–285.
[21] M. Tonelli, G. Paglietti, V. Boido, F. Sparatore, F. Marongiu, E. Marongiu, P. La Colla, R. Loddo, *Chem. Biodivers*. **2008**, *5*, 2386–2401.
[22] M. Alp, H. Goker, R. Brun, S. Yıldız, *Eur. J. Med. Chem*. **2009**, *44*, 2002–2008.
[23] S. Demirayak, U. Abu Mohsen, A. Cagri Karaburun, *Eur. J. Med. Chem*. **2002**, *37*, 255–260.
[24] a) A. S. Alpan, H. S. Gunes, Z. Topcu, *Acta. Biochim. Pol*. **2007**, *54*, 561–565. b) A. S. Alpan, S. Zencir, I. Zupkó, G. Coban, B. Réthy, H. S. Gunes, Z. Topcu, *J. Enzyme. Inhib. Med. Chem*. **2009**, *24*, 844–849.
[25] a) A. S. Alpan, S. Parlar, L. Carlino, A. H. Tarikogullari, V. Alptüzün, H. S. Günes, *Bioorg. Med. Chem*. **2013**, *21*, 4928–4937. b) G. Coban, L. Carlino, A. H. Tarikogullari, S. Parlar, G. Sarıkaya, V. Alptüzün, A. S. Alpan, H. S. Günes, E. Erciyas, *Med. Chem. Res*. **2016**, *25*, 2005–2014. c) J. Zhu, C. Wu, X. Li, G. Wu, S. Xie, Q. Hu, Z. Deng, M. X. Zhu, H. Luo, X. Hong, *Bioorg. Med. Chem*. **2013**, *21*, 4218–4224. d) Y. K. Yoon, M. A. Ali, A. C. Wei, T. S. Choon, K. Khaw, V. Murugaiyah, H. Osman, V. H. Masand, *Bioorg. Chem*. **2013**, *49*, 33–39.
[26] G. Roman, *Eur. J. Med. Chem*. **2015**, *89*, 743–816.
[27] M. Rehman, M. Imran, M. Arif, M. Farooq, *World Appl. Program*. **2013**, *3*, 558–564.
[28] H. I. Gul, Z. Yazici, M. Tanc, C. T. Supuran, *J. Enzyme. Inhib. Med. Chem*. **2016**, *31*, 1540–1544.
[29] P. N. Preston, in *The Chemistry of Heterocyclic Compounds*: Benzimidazoles and congeneric tricyclic

compounds (Eds: A. Weissberger, E. C. Taylor), John & Wiley Sons, New York 1981, part 1, vol. 40, p. 63–64.
[30] R. M. Silverstein, G. C. Bassler, T. C. Morrill, *Spectrometric Identification of Organic Compounds*, 4th edn., John Wiley & Sons, New York **1981**, chapter 3.
[31] V. Sridharan, S. Saravanan, S. Muthusubramanian, S. Sivasubramanian, *Magn. Reson. Chem*. **2005**, *43*, 551–556.
[32] G. L. Ellman, K. D. Courtney, V. Andres, R. M. Featherstone, *Biochem. Pharmacol*. **1961**, *7*, 88–90.
[33] S. Chen, L. Zou, L. Li, T. Wu, *PLoS ONE* **2013**, *8*, e53662.
[34] N. Gharavi, S. Haggarty, A. O. El-Kadi, *Curr. Drug. Metab*. **2007**, *8*, 1–7.
[35] S. Olgen, Z. Kilic, A. O. Ada, T. Coban, *J. Enzyme Inhib. Med. Chem*. **2007**, *22*, 457–462.
[36] O. H. Lowry, N. J. Rosenbrough, A. L. Farr, R. J. Randall, *J. Biol. Chem*. **1951**, *193*, 265–375.
[37] H. H. Draper, M. Hadley, *Methods Enzimol*. **1990**, *186*, 421–431.
[38] A. Santamaría, S. Galván-Arzate, V. Lisý, S. F. Ali, H. M. Duhart, L. Osorio-Rico, C. Ríos, F. St'astný, *Neuroreport* **2001**, *12*, 871–874.
[39] K. Arnold, L. Bordoli, J. Kopp, T. Schwede, *Bioinformatics* **2006**, *22*, 195–201.
[40] P. Benkert, M. Biasini, T. Schwede, *Bioinformatics* **2011**, *27*, 343–350.
[41] V. Hornak, R. Abel, A. Okur, B. Strockbine, A. Roitberg, C. Simmerling, *Proteins: Struct. Funct. Bioinf*. **2006**, *65*, 712–725.
[42] W. L. Jorgensen, J. Chandrasekhar, J. D. Madura, *J. Chem. Phys*. **1983**, *79*, 926–935.
[43] D. A. Case, T. A. Darden, T. E. Cheatham, C. L. Simmerling, J. Wang, R. E. Duke, R. Luo, R. C. Walker, W. Zhang, K. M. Merz, B. Roberts, S. Hayik, A. Roitberg, G. Seabra, J. Swails, A. W. Goetz, I. Kolossváry, K. F. Wong, F. Paesani, J. Vanicek, R. M. Wolf, J. Liu, X. Wu, S. R. Brozell, T. Steinbrecher, H. Gohlke, Q. Cai, X. Ye, J. Wang, M. J. Hsieh, G. Cui, D. R. Roe, D. H. Mathews, M. G. Seetin, R. Salomon-Ferrer, C. Sagui, V. Babin, T. Luchko, S. Gusarov, A. Kovalenko, P. A. Kollman, *Amber* 12, **2012**.
[44] Molecular Operating Environment (MOE 2014.09) Chemical Computing Group Inc., 1010 Sherbrooke Street West, Suite 910, Montreal H3A 2R7, Canada.
[45] T. A. Halgren, *J. Comput. Chem*. **1996**, *17*, 490–519.
[46] G. Jones, P. Willett, R. C. Glen, *J. Mol. Biol*. **1995**, *245*, 43–53.
[47] G. Jones, P. Willett, R. C. Glen, A. R. Leach, R. Taylor, *J. Mol. Biol*. **1997**, *267*, 727–748.
[48] A. Jakalian, B. L. Bush, D. B. Jack, *J. Comput. Chem*. **2000**, *21*, 132–146.
[49] J. Wang, R. M. Wolf, J. W. Caldwell, P. A. Kollman, D. A. Case, *J. Comput. Chem*. **2004**, *25*, 1157–1174.
[50] J. P. Ryckaert, G. Ciccotti, H. J. C. Berendsen, *J. Comput. Phys*. **1977**, *23*, 327–341.
[51] U. Essmann, L. Perera, M. L. Berkowitz, T. Darden, H. Lee, L. G. Pedersen, *J. Chem. Phys*. **1995**, *103*, 8577–8593.
[52] Grace Development Team, http://plasma-gate.weizmann.ac.il/Grace/
[53] D. R. Roe, T. E. Cheatham, *J. Chem. Theory Comput*. **2013**, *9*, 3084–3095.
[54] F. Fabiola, R. Bertram, A. Korostelev, M. S. Chapman, *Protein Sci*. **2002**, *11*, 1415–1423.
[55] E. F. Pettersen, T. D. Goddard, C. C. Huang, G. S. Couch, D. M. Greenblatt, E. C. Meng, T. E. Ferrin, *J. Comput. Chem*. **2004**, *13*, 1605–1612.
[56] S. A. Wildman, G. M. Crippen, *J. Chem. Inf. Comput. Sci*. **1999**, *39*, 868–873.